The eyelid and pupil dynamics underlying stress levels in awake mice.

Hang Zeng [1,2].

[1]High-Field Magnetic Resonance Department, Max Planck Institute for Biological Cybernetics, Tübingen, Germany.

[2]Present address: Department of Medical Biochemistry and Biophysics | Karolinska Institutet Solnavägen 9, 171 77 Stockholm.

Correspondence and requests for materials should be addressed to:

Dr Hang Zeng: zenghang@yeah.net.

Abstract

Stress is a natural response of the body to perceived threats, and it can have both positive and negative effects on brain hemodynamics. Stress-induced changes in pupil and eyelid size/shape have been used as a biomarker in several fMRI studies. However, there were limited knowledges regarding changes in behavior of pupil and eyelid dynamics, particularly on animal models. In the present study, the pupil and eyelid dynamics were carefully investigated and characterized in a newly developed awake rodent fMRI protocol. Leveraging deep learning techniques, the mouse pupil and eyelid diameters were extracted and analyzed during different training and imaging phases in the present project. Our findings demonstrate a consistent downwards trend in pupil and eyelid dynamics under a meticulously designed training protocol, suggesting that the behaviors of the pupil and eyelid can be served as reliable indicators of stress levels and motion artifacts in awake fMRI studies. The current recording platform not only enables the facilitation of awake animal MRI studies but also highlights its potential applications to numerous other research areas, owing to the non-invasive nature and straightforward implementation.

Introduction

The awake mouse model, under normal or pathological conditions, has been widely used in functional magnetic resonance imaging (fMRI) as a platform for investigating various physiological activities, e.g., brain fluctuations[1-3], behavior[4], cognition processing[5, 6]. Thus, laying a solid foundation for translational studies from basic brain research to the clinical applications. Nowadays, numerous neuroimaging laboratories are working on developing awake animal models for their fMRI protocols. However, one significant challenge needs to be carefully considered, i.e., the potential stress caused to the animals during the imaging procedures, which can severely affect physiological states and brain hemodynamic activities. In previous studies, researchers have utilized various methods to measure stress levels in rodents, such as plasma corticosterone levels[2], changes in blood pressure, respiration rate or heat rate[7-9], etc. Though those measurements can be applied, it is still crucial to consider the limitations and potential confounding factors of each method when applying to the awake animals, particularly for awake fMRI protocols. As a results, many labs are exploring alternative approaches, such as pupillometry and eyelid dynamics, which are non-invasive and effective methods for stress level monitoring [3, 10].

Previous studies have demonstrated the relationship between stress and pupil dynamic[11]. One study found that pupils of individuals exposed to stress-inducing stimuli, such as a loud noise or electric shock, dilated more than pupils exposed to non-stressful stimuli[12]. Another study found that the pupils of individuals with post-traumatic stress disorder (PTSD) were more likely to remain dilated than those without PTSD, indicating a persistent stress response[13]. In addition to pupillometry dynamics, eyelid dynamics have also been proposed as a promising biomarker of stress in both humans and animals. For example, one study found that

individuals with high levels of anxiety and stress exhibited increased blink rates and reduced eyelid closure duration[14]. Previous studies have reported eyelid behaviors, i.e., closure, open, and blinking, etc., have been linked with brain fluctuations[15-18]. The eyelid closures were reported be to link with the brain arousal state[15]. Whereas eye-blinking events were found related to cortical fluctuations[18]. Furthermore, the eyelid closures and openings modulate brain functional connectivity, showing different temporal properties of brain networks[19].

The pupil and eyelid behaviors conveying massive information flows, have been applied as the physiological tenants to underlie the stress levels. Nonetheless, the significant pupillometry dynamics and eyelid behavioral states lack a precise evaluation for encoding stress levels. Here, in the current project, we aim to non-invasively investigate the possible link between MRI-induced stress levels and pupil/eyelid dynamics on an awake mouse model, including how the pupil/eyelid changes in size and shape occur in response to stress, and how these changes, particularly, the the dynamic temporal features, can be utilized to evaluate the stress levels in building the awake fMRI protocols. By comprehensively characterizing the pupil/eyelid dynamics and their relationship with stress levels, we seek to provide a novel and reliable approach for assessing stress in awake animal imaging modalities, and establish the validity and reliability of this approach with potential applications in both preclinical research and clinical practice.

Material and methods

Animals and habituation

7 male C57BL/6 mice (Charles River Laboratory) were trained in this project. Animals were habituated individually at a 12 hr-12 hr light-dark cycle (light on from 8 a.m. to 8 p.m.) with food and water ad libitum, starting at age 10-15 weeks. All the surgical and imaging procedures were approved by the state authority (Regierungspräsidium, Tübingen, Baden-Württemberg, Germany) and conducted in full accordance with the German Animal Welfare Act (TierSchG) and Animal Welfare Laboratory Animal Ordinance (TierSchVersV).

All the animals were trained 5-8 weeks for the awake MR imaging. The animals' head was fixed, and the body left unrestrained within the training apparatus. Only the well-trained animals were applied in further imaging. The acclimating procedures were depicted in our previous report[20].

Head-post surgery

Mice were anesthetized by isoflurane (2% for induction; 1-1.3% for surgery in a mixture of 30% oxygen in air) and fixed in a stereotaxic frame. The customized head-post was printed out using our 3D printer(From 2, www.formlabs.com). We applied dental cement (Charisma flow) to fix the head-post on top of the skull. Painkillers and antibiotics were administered to relieve pain and inflammation immediately after finishing the surgery. Animals were maintained on a heated blanket until fully recovered from the anesthetic effect (15-30 mins) and were placed back in their original cages. Post-surgical observations were documented for a minimum of five consecutive days following the surgery (twice a day for five days and then daily). Detailed surgical procedures can be found in our previous reports.

106 ***Eyelid/pupil acquisition***

107 A customized MRI-compatible camera with infra light (850 nm) was specially
108 designed and applied for eyelid tracking and pupillometry recording in this study.
109 Under iso-/luminance, the pupil and eyelid videos (32 bites/pixel, with a resolution
110 of 1920×1080 pixel and refresh rate of 60 frames/s) were continuously recorded
111 from left eye of the mouse.

112

113 The camera was mounted in an adjustable non-magnetic holder for consistence of
114 MRI scanner. The animals were head-fixed and positioned ~0.8 cm away from the
115 camera in the restraining apparatus. The eyelid/pupil video recordings were started
116 simultaneously with the initial of MR imaging.

117

118 ***fMRI data acquisition***

119 The fMRI datasets were acquired using a Bruker Avance III System (Bruker BioSpin,
120 Ettlingen, Germany) with a 14.1-T superconducting magnet with a 12 cm diameter
121 gradient providing 100 G/cm with a 150 μs rise time. A custom-made transceiver
122 surface coil (8 mm in diameter) covering the whole brain of mice was applied for
123 imaging. Functional scans and anatomical images were acquired using the 2D echo-
124 planar imaging (EPI, 24 slices, 0.3×0.3×0.5 mm^3 resolution) and rapid acquisition
125 with relaxation enhancement sequences (RARE, 24 slices, 0.125 mm^2 in-plane
126 resolution, 0.5 mm slice thickness) sequences, respectively. All the fMRI datasets
127 were preprocessed by using the Analysis of Functional NeruoImage (AFNI)
128 software package (https://afni.nimh.nih.gov/)[21].

129

130 ***Data analysis***

131 The coordinates of eyelid/pupil were automatically labeled and extracted using the
132 DeepLabCut [22, 23] network. To establish this network, 37 raw videos were applied

and trained in the current study. Basically, 100 frames/video were chosen and labeled for training the network (8 points per frames, i.e., right, left, up, bottom boundary of eyelid and pupil, respectively). The algorithm for measuring the diameter of eyelid (ED) and pupil(PD) is as following[3, 24]:

$$ED = \frac{1}{2} \times \left(\sqrt{(a_2 - a_1)^2 + (b_2 - b_1)^2} + \sqrt{(a_4 - a_3)^2 + (b_4 - b_3)^2} \right)$$

$$PD = \frac{1}{2} \times \left(\sqrt{(x_2 - x_1)^2 + (y_2 - y_1)^2} + \sqrt{(x_4 - x_3)^2 + (y_4 - y_3)^2} \right)$$

Where the coordinates of the points (a_i, b_i), i = 1, ..., 4 and (x_j, y_j), j = 1, ..., 4, were used to calculate the ED and PD, respectively.

The anatomical MR image qualities were assessed by comparing the SNR (signal-to-noise-ratio) between the different time points extracted from the training datasets. The formular of SNR is as following[25]:

$$SNR_k = \frac{SI_k}{\sigma}$$

where SI_k stands for mean of signal intensity in the regions of interest (ROIs) labeled by k, and σ denotes the standard deviation of background signal intensity outside the ROI. We manually selected the corpus callosum (close to the surface and shows less distortion) as the ROI to represent the whole brain image and calculate the signal intensity.

Statistical analysis

All data are shown as mean ± SEM. Statistical analyses were performed in python or GraphPad Prism version 9, and all figures were generated in python and GraphPad.

Results

Experimental design

Figure 1 shows the schematics of the awake mouse eyelid and pupillometry recordings, as well as the training system and MR imaging modules. Figure 1A depicts the experimental designs of the animal, undergoing headpost implantation, restraint training, and fMRI imaging, etc. The experimental procedures matching to the training and imaging steps were shown in Fig.1B, e.g., a plastic headpost was firstly, implanted and then trained in the customized apparatus, and finally, went for imaging in MR scanners. Fig.1C shows the eyelid and pupil diameter were recorded and extracted for analysis. The functional and anatomical MR images were also obtained when the animals were trained ready for imaging.

Pupil dynamics

Figure 2 shows the pupillometry dynamics during the training period. Of which, Fig.2A displays the mean pupil diameter from all the recorded trails in different training sections. Moreover, the pupil diameter correlated with the training period, showing a decline trend towards the end of restraining section (linear regression, R^2=0.55, p<0.01). Further analysis revealed significant changes of the pupillometry following the implemented training protocol, i.e., earlier phases (1-3 week) vs. later phases (4 -11 week), showing reduced pupillometry dynamics (Fig.2B, p<0.01). These results may suggest that the animals get accustomed to the training and show less stress to the restraint apparatus. It thus, further validates the current awake mouse MRI platform for brain imaging.

Eyelid dynamics

Similarly, the eyelid dynamics from every individual animal were extracted through our trained DeepLab Cut network. The average eyelid diameter across all training

183 sections were graphically represented as a function of time, as illustrated in Fig.3A,
184 which revealed that later training sections had fewer alterations. Moreover, a linear
185 regression analysis was also conducted to assess the changes in eyelid dynamics,
186 which yielded a coefficient of determination (R^2) value of 0.64 ($p<0.01$), indicating
187 a significant decline in eyelid dynamics. Further statistical analysis verified the
188 identical findings of a smaller eyelid dynamics in the late stage (5-11 week) of
189 training in comparison to the early stage (1-4 week) of training (Fig.3B, $p<0.01$).
190 These findings imply that the animals, after intensive training in the MR apparatus,
191 became habituated to the imaging environment and showed decreased discomfort.
192
193 ***SNR analysis of the MR images***
194 Next the MR image quality were also quantified by calculating the SNRs from
195 different training stages when the brain images were acquired. As depicted in Fig.4A,
196 the SNR values pertaining to the spatial MR images exhibited a gradual
197 improvement throughout the training periods, indicative of a progressive upward
198 trend towards the training phase ($R^2=0.71$, $p<0.05$). Further analysis suggested that
199 the SNR of the MR images acquired were better in the late stage (7-11 week) than
200 early stage (1-6 week) (Fig.4B, $p<0.05$). The observed augmentation in SNR for the
201 MR images implies a reduction in motion artifacts during the image acquisition
202 process, thus signifying a diminished level of stress and discomfort of the animals.
203
204
205
206

Discussion

Pupillometry, a technique that measures the pupil's size and dynamics to assess the cognitive, mental demands and arousing state levels, etc., in individuals that has long been investigated for over 50 years[26]. Nowadays, it has led to the development of various methods for measuring stress levels for both human subjects and animal models. The current study, by applying the deep neural networks, not only presents the dynamics changes of pupillometry, but also shed light on the dynamics of eyelid for monitoring the physical stress on an awake mouse model, particularly, during the fMRI imaging modalities. Making it a valuable tool to non-invasively assess the stress levels and cognitive overload in individuals with potential applications for future preclinical researh and clinical practice.

The animals in the current study were consciously being exposed to such an acoustic environment (>100 dB, produced by the scanner) and were kept still without movements. It is thus impossible for the animals to avoid the physical stress induced by the imaging apparatus. To mimic the stress-induced changes in brain hemodynamics, we have applied a new awake training protocol and kept measuring the pupil diameter changes throughout the entire experiment. Our findings proved that with proper training procedures and exposure periods, the animals' training effects can be visualized and quantified as indicated by the pupillometry measurement in a real-time manner. Instead of measuring corticosterone level or recording respiration/heart rate as the stress biomarkers, we assessed the dynamic changes of the pupil due to its non-invasive and non-physical contact to the conscious animals. Furthermore, stress-induced changes in pupil size and shape have been suggested to be resulted from the activation of the autonomic nervous system's sympathetic branch[27, 28]. Therefore, the pupillometry, on the one hand reflects the stress levels during training, and on the other hand, indicates the activities of the

sympathetic nervous system while imaging. Ensuring the examiners to perform longitudinal studies and to explore the brain hemodynamics underlying behavior or disease states with limited stress-induced effects in a controlled laboratory setting.

The use of eyelid dynamics to assess the stress-induced effects has been reported in previous studies[29]. However, very few studies have focused on the eyelid dynamics and the examination of eyelid dynamics as a potential stress biomarker remains largely unexplored. Though, preliminary findings suggest that increased blink rates[30], shorter durations of blinks[15], and enhanced eyelid closure velocity[15, 31] were all related to higher levels of stress. However, these results underestimated the potential applications of eyelid dynamics as a promising stress biomarker. In the current investigations, we dynamically retrieved and analysed the changes in eyelid diameter on a mouse model, revealing a substantial link between stress levels and changes in eyelid dynamics, particularly during training and imaging for fMRI modalities. Our analysis indicated that the eyelid dynamics provide significant valuable insights between the earlier and later phases of training/imaging modules, offering a non-invasive and objective insights into the stress-induced response on awake animal models.

In conclusion, this study sheds light on the relationships between stress level and pupil & eyelid dynamics, highlighting the potential applications of pupil and eyelid dynamics as a non-invasive and objective stress biomarker. By monitoring the pupil and eyelid diameter changes, researchers and clinicians can potentially identify and measure stress levels in real-time, enhancing the accuracy and efficiency of stress assessment. Our findings may also provide a step toward understanding of the complex interplay between stress and human behavior, which might revolutionize stress assessment and contribute to the development of personalized stress

management strategies in various domains, including healthcare, occupational settings, and mental well-being, etc.

Limitations of the study

Overall, measuring stress levels in awake animals is essential, not only for ensuring well-being of the animals, but also critical for investigators to produce reliable and repeatable results. We have proposed to measure the dynamics of the pupil and eyelid as the biomarkers for stress evaluations. However, there are several limitations that must be considered. One of the main limitations is that the pupil and eyelid dynamic data were recorded in a controlled, specific fMRI lab settings. Such a constraint and noisy environment may not only induce physical stress to the conscious animals, but also might be psychological-associated as well. It may vary depending on the examiners' experimental surroundings. Another limitation is the lack of standardization between the stress levels and the dynamics of pupil and eyelid. By real-time monitoring the diameter changes of pupil and eyelid, the stress-induced effects can be detected. However, to what extent this effect can be indicative and interpretable remains ambiguous, particularly on awake animal models. Finally, the pupil and eyelid are not a perfect circle, and its shape and position can be affected by changes in the iris's curvature and illuminations. Future investigations may focus more on developing new analytical methods as well as the implementation of well-designed experiments.

Acknowledgements

We thank Miss. Gao for processing the raw videos and providing analytical comments.

Author contributions

Dr. Zeng and Miss. Gao were responsible for the data analysis as well as the preparation of the manuscripts.

Funding

No fundings.

Competing interests

The authors declare no competing interests.

298 # Reference

299 1. Gutierrez-Barragan D, Singh NA, Alvino FG, Coletta L, Rocchi F, De
300 Guzman E, Galbusera A, Uboldi M, Panzeri S, Gozzi A: **Unique**
301 **spatiotemporal fMRI dynamics in the awake mouse brain**. *Curr Biol* 2022,
302 **32**(3):631-644 e636.
303 2. Tsurugizawa T, Tamada K, Ono N, Karakawa S, Kodama Y, Debacker C,
304 Hata J, Okano H, Kitamura A, Zalesky A *et al*: **Awake functional MRI**
305 **detects neural circuit dysfunction in a mouse model of autism**. *Sci Adv*
306 2020, **6**(6):eaav4520.
307 3. Zeng H, Jiang Y, Beer-Hammer S, Yu X: **Awake Mouse fMRI and**
308 **Pupillary Recordings in the Ultra-High Magnetic Field**. *Front Neurosci*
309 2022, **16**:886709.
310 4. Han Z, Chen W, Chen X, Zhang K, Tong C, Zhang X, Li CT, Liang Z: **Awake**
311 **and behaving mouse fMRI during Go/No-Go task**. *Neuroimage* 2019,
312 **188**:733-742.
313 5. Harris AP, Lennen RJ, Marshall I, Jansen MA, Pernet CR, Brydges NM,
314 Duguid IC, Holmes MC: **Imaging learned fear circuitry in awake mice**
315 **using fMRI**. *Eur J Neurosci* 2015, **42**(5):2125-2134.
316 6. Chen X, Tong C, Han Z, Zhang K, Bo B, Feng Y, Liang Z: **Sensory evoked**
317 **fMRI paradigms in awake mice**. *Neuroimage* 2020, **204**:116242.
318 7. Duong TQ: **Cerebral blood flow and BOLD fMRI responses to hypoxia in**
319 **awake and anesthetized rats**. *Brain Res* 2007, **1135**(1):186-194.
320 8. Fadel LC, Patel IV, Romero J, Tan IC, Kesler SR, Rao V, Subasinghe S, Ray
321 RS, Yustein JT, Allen MJ *et al*: **A Mouse Holder for Awake Functional**
322 **Imaging in Unanesthetized Mice: Applications in (31)P Spectroscopy,**
323 **Manganese-Enhanced Magnetic Resonance Imaging Studies, and**

Resting-State Functional Magnetic Resonance Imaging. *Biosensors (Basel)* 2022, **12**(8).

9. Dinh TNA, Jung WB, Shim HJ, Kim SG: **Characteristics of fMRI responses to visual stimulation in anesthetized vs. awake mice**. *Neuroimage* 2021, **226**:117542.

10. Lellakova M, Pavlak A, Leskova L, Florian M, Skurkova L, Mesarcova L, Kottferova L, Takacova D, Kottferova J: **Monitoring Blinks And Eyelid Twitches In Horses To Assess Stress During The Samples Collection Process**. *J Appl Anim Welf Sci* 2021:1-10.

11. Bertilsson J, Niehorster DC, Fredriksson PJ, Dahl M, Graner S, Fredriksson O, Martensson JM, Magnusson M, Fransson PA, Nystrom M: **Stress Levels Escalate When Repeatedly Performing Tasks Involving Threats**. *Front Psychol* 2019, **10**:1562.

12. Bradley MM, Miccoli L, Escrig MA, Lang PJ: **The pupil as a measure of emotional arousal and autonomic activation**. *Psychophysiology* 2008, **45**(4):602-607.

13. Cascardi M, Armstrong D, Chung L, Pare D: **Pupil Response to Threat in Trauma-Exposed Individuals With or Without PTSD**. *J Trauma Stress* 2015, **28**(4):370-374.

14. Mott RO, Hawthorne SJ, McBride SD: **Blink rate as a measure of stress and attention in the domestic horse (Equus caballus)**. *Sci Rep* 2020, **10**(1):21409.

15. Wang C, Ong JL, Patanaik A, Zhou J, Chee MW: **Spontaneous eyelid closures link vigilance fluctuation with fMRI dynamic connectivity states**. *Proc Natl Acad Sci U S A* 2016, **113**(34):9653-9658.

349 16. Ong JL, Asplund CL, Chia TTY, Chee MWL: **Now You Hear Me, Now You**
350 **Don't: Eyelid Closures as an Indicator of Auditory Task Disengagement**.
351 *Sleep* 2013, **36**(12):1867-1874.
352 17. Chung JY, Yoon HW, Song MS, Park H: **Event related fMRI studies of**
353 **voluntary and inhibited eye blinking using a time marker of EOG**.
354 *Neuroscience Letters* 2006, **395**(3):196-200.
355 18. Guipponi O, Odouard S, Pinede S, Wardak C, Ben Hamed S: **fMRI Cortical**
356 **Correlates of Spontaneous Eye Blinks in the Nonhuman Primate**.
357 *Cerebral Cortex* 2015, **25**(9):2333-2345.
358 19. Weng Y, Liu X, Hu H, Huang H, Zheng S, Chen Q, Song J, Cao B, Wang J,
359 Wang S *et al*: **Open eyes and closed eyes elicit different temporal**
360 **properties of brain functional networks**. *Neuroimage* 2020, **222**:117230.
361 20. Zeng H, Jiang Y, Beer-Hammer S, Yu X: **Awake Mouse fMRI and**
362 **Pupillary Recordings in the Ultra-High Magnetic Field**. *Front Neurosci-*
363 *Switz* 2022, **16**.
364 21. Cox RW: **AFNI: software for analysis and visualization of functional**
365 **magnetic resonance neuroimages**. *Comput Biomed Res* 1996, **29**(3):162-
366 173.
367 22. Nath T, Mathis A, Chen AC, Patel A, Bethge M, Mathis MW: **Using**
368 **DeepLabCut for 3D markerless pose estimation across species and**
369 **behaviors**. *Nature Protocols* 2019, **14**(7):2152-2176.
370 23. Mathis A, Mamidanna P, Cury KM, Abe T, Murthy VN, Mathis MW, Bethge
371 M: **DeepLabCut: markerless pose estimation of user-defined body parts**
372 **with deep learning**. *Nat Neurosci* 2018, **21**(9):1281-1289.
373 24. Pais-Roldan P, Takahashi K, Sobczak F, Chen Y, Zhao X, Zeng H, Jiang Y,
374 Yu X: **Indexing brain state-dependent pupil dynamics with simultaneous**

375 **fMRI and optical fiber calcium recording**. *Proc Natl Acad Sci U S A* 2020,
376 **117**(12):6875-6882.
377 25. Goerner FL, Clarke GD: **Measuring signal-to-noise ratio in partially**
378 **parallel imaging MRI**. *Med Phys* 2011, **38**(9):5049-5057.
379 26. Hess EH: **Attitude and Pupil Size**. *Sci Am* 1965, **212**:46-54.
380 27. Slavik O, Horky P, Velisek J, Valcharova T: **Pupil size variation as a**
381 **response to stress in European catfish and its application for social stress**
382 **detection in albino conspecifics**. *PLoS One* 2020, **15**(12):e0244017.
383 28. Sato F, Laeng B, Nakauchi S, Minami T: **Cueing the Necker cube: Pupil**
384 **dilation reflects the viewing-from-above constraint in bistable perception**.
385 *J Vis* 2020, **20**(4):7.
386 29. Merkies K, Ready C, Farkas L, Hodder A: **Eye Blink Rates and Eyelid**
387 **Twitches as a Non-Invasive Measure of Stress in the Domestic Horse**.
388 *Animals (Basel)* 2019, **9**(8).
389 30. Korda AI, Giannakakis G, Ventouras E, Asvestas PA, Smyrnis N, Marias K,
390 Matsopoulos GK: **Recognition of Blinks Activity Patterns during Stress**
391 **Conditions Using CNN and Markovian Analysis**. *Signals* 2021, **2**(1):55-71.
392 31. Joseph Antony S: **Imaging shear stress distribution and evaluating the**
393 **stress concentration factor of the human eye**. *Sci Rep* 2015, **5**:8899.
394

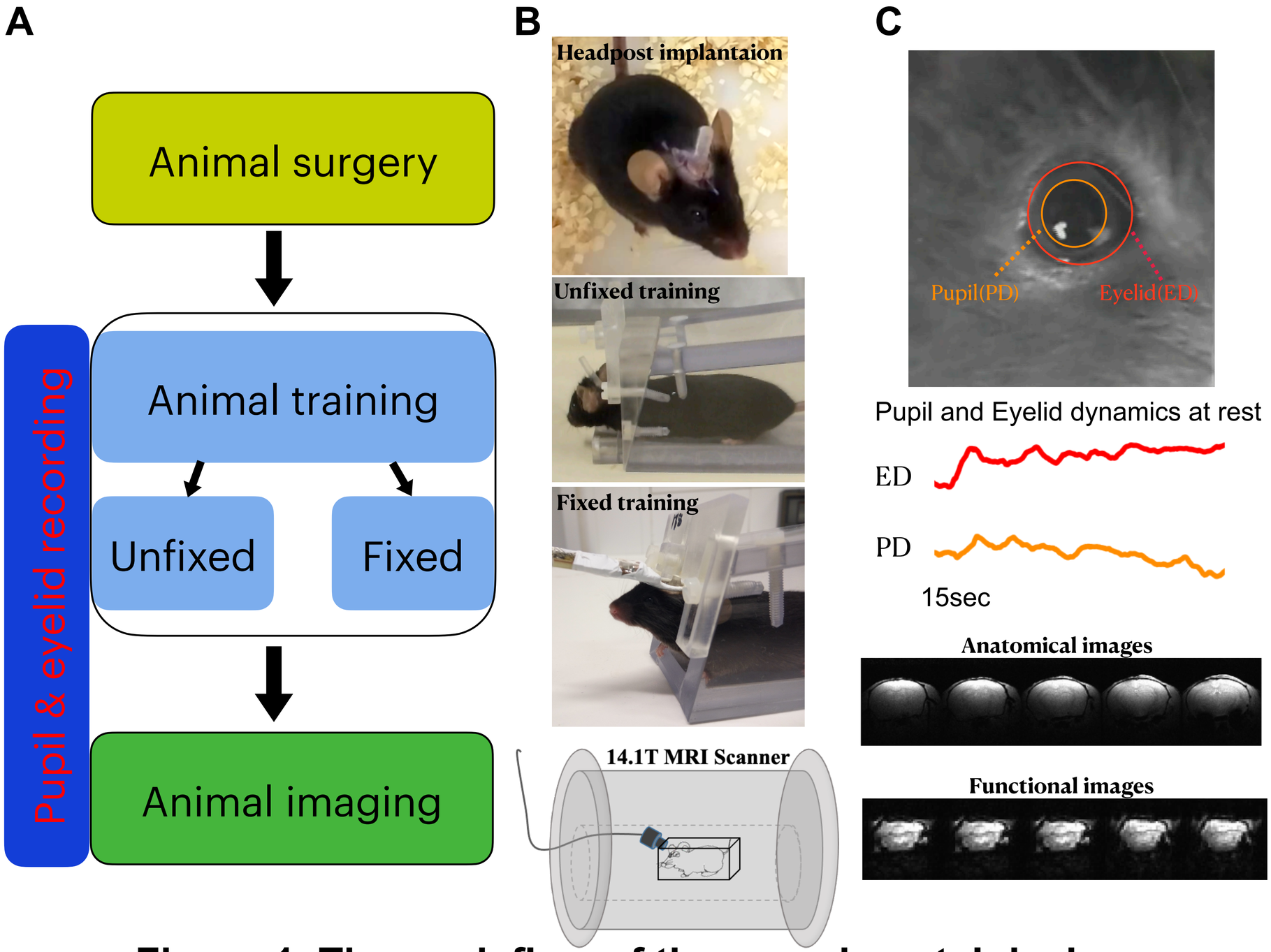

Figure 1. The work flow of the experimental designs

Figure 1. The work flow of the experimental designs. Fig.1A depicts the experimental designs of the animal, undergoing headpost implantation, training, and MRI imaging. Fig.1B shows the experimental demos matching to the experimental techniques in Fig.1A. Fig.1C is a representative trial of the eyelid and pupil recordings and MR images.

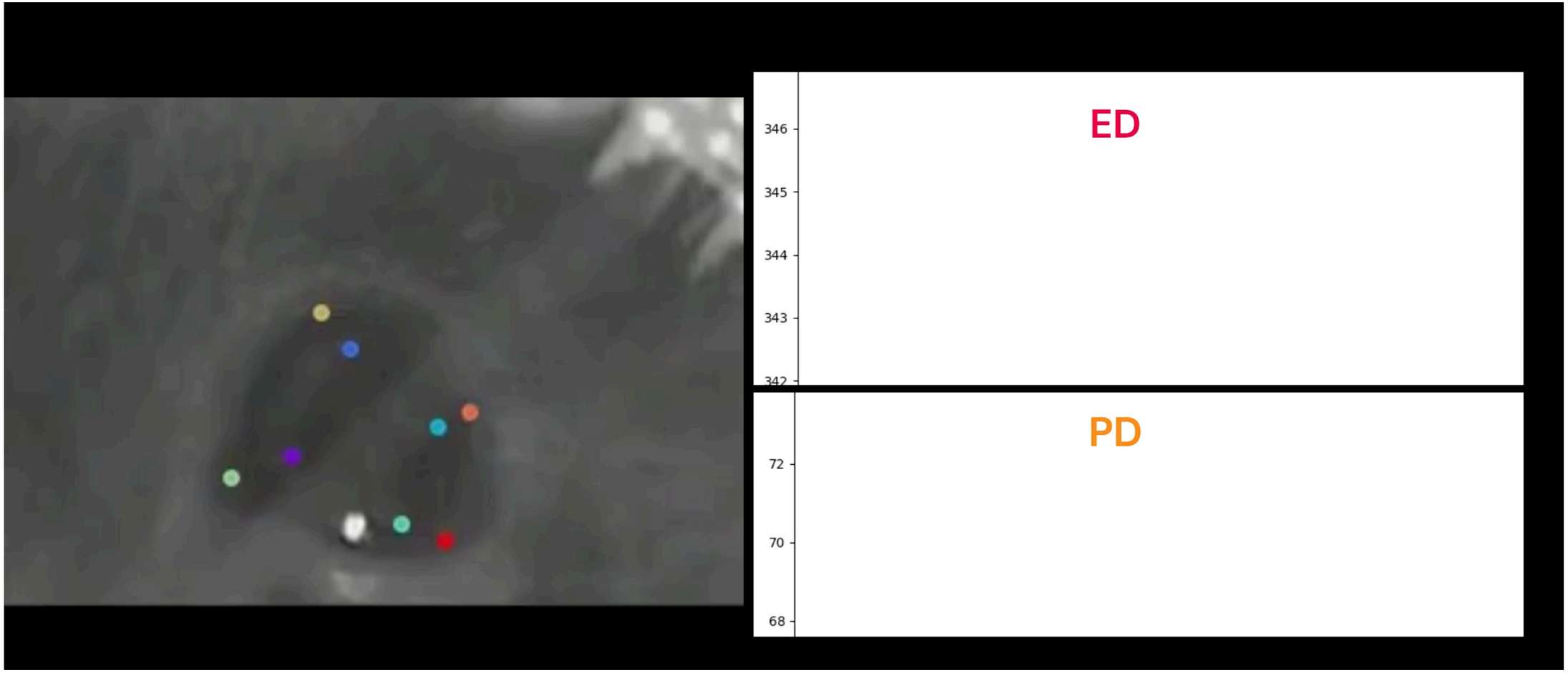

Supplementary video S1. The left video shows the labeled pupil and eyelid dynamics, and the right video shows the corresponding timecourses of eyelid dynamics (ED) and pupil dynamics (PD).

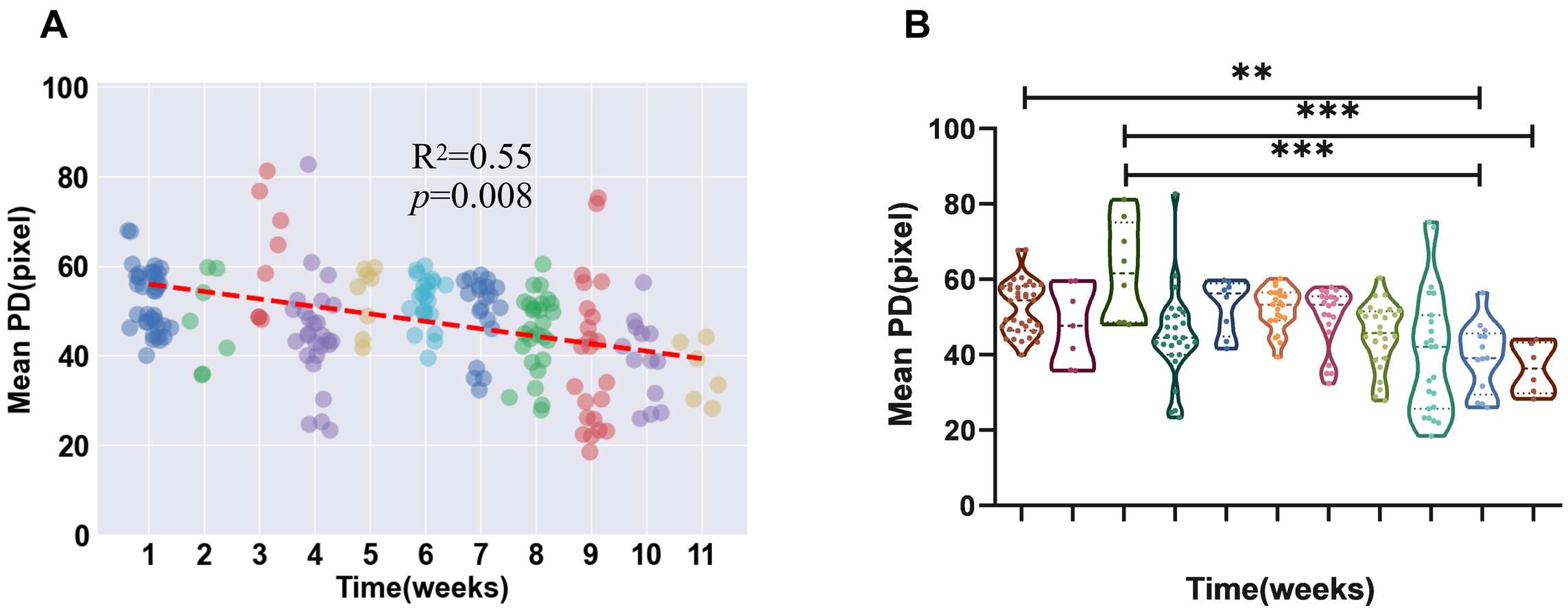

Figure 2. Pupil dynamic changes following the training weeks. Fig.2A shows the scatter plot of the mean pupil dynamics and the linear regression of those plots following the training periods. Red line denotes the trend of the changes for the pupil. Fig.2B shows the statistical analysis of the mean pupil diameters among the different weeks (mean±S.E.M, one-way ANOVA, ***p<0.001, Bonferroni post hoc test).

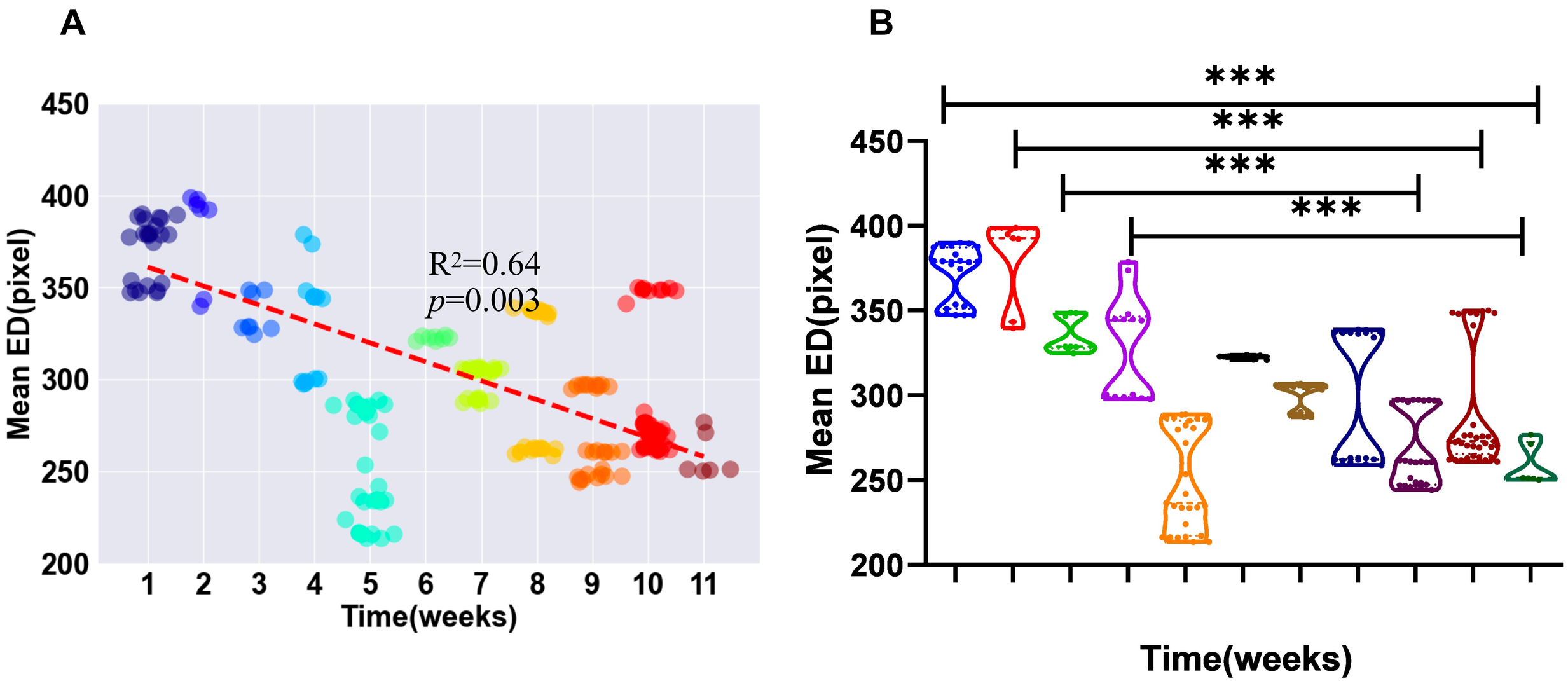

Figure 3. Eyelid dynamic changes following the training weeks.

Figure 3. Eyelid dynamic changes following the training weeks. Fig.3A shows the scatter plot of the mean eyelid dynamics and the linear regression of those plots following differnent training periods. Red line denotes the trend of the changes for the eyelid diameters. Fig.3B shows the statistical analysis of the mean eyelid diameters among the different weeks (mean±S.E.M, one-way ANOVA, ***$p<0.001$, Bonferroni post hoc test).

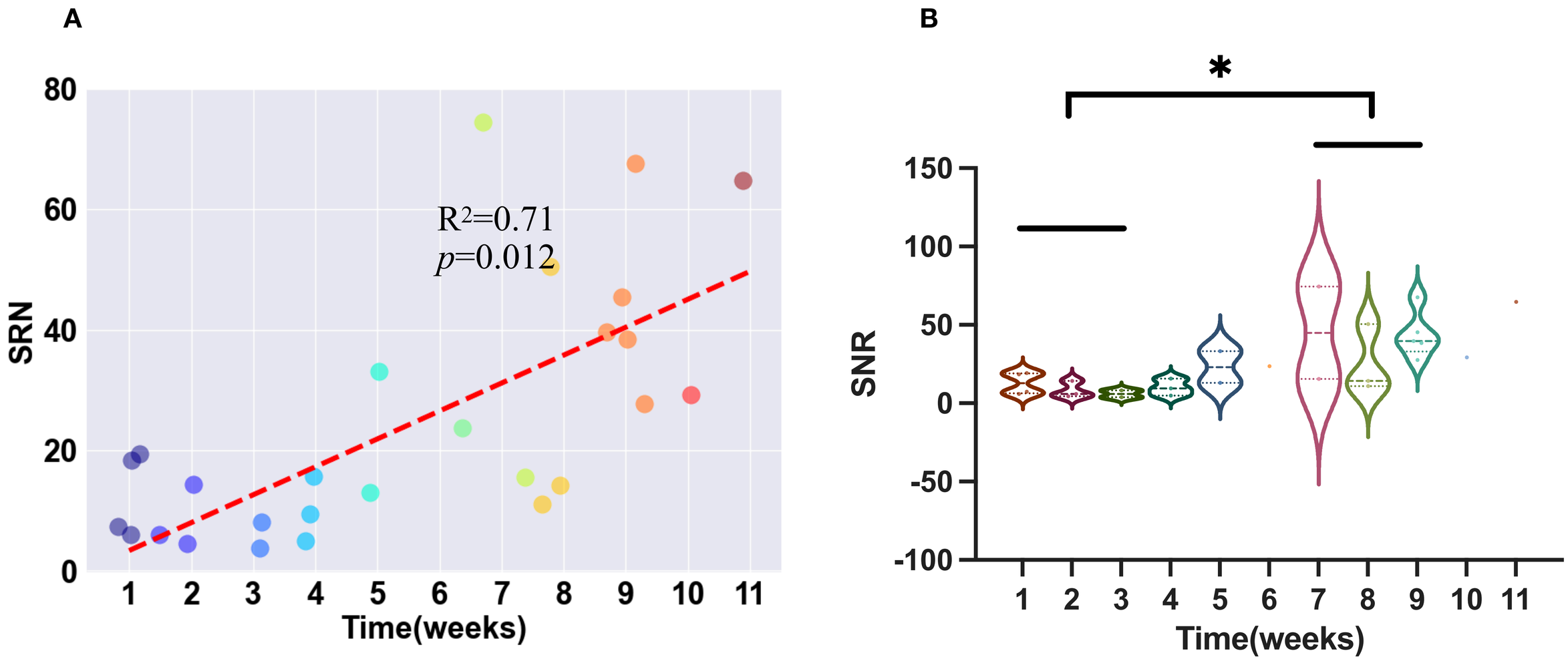

Figure 4. The SNR of the MRI scans among the different weeks of training

Figure 4. The SNR of the MRI scans among the different weeks of training. Fig.4A shows the scatter plot of the mean SNR values and the linear regression of those plots at different weeks of training. Red line denotes the trend of changes for SNR. Fig.4B shows the statistical analysis of the SNR values among the different weeks (mean±S.E.M, one-way ANOVA, *$p<0.05$, Bonferroni post hoc test).

Summary of non-human(primates) awake fMRI since year 2000

Ref.	Scanner	Species	Anesthetics	Training	Setups	Ear/Bite bar	Stress monitor	Motion detection	Stimulus
(Gutierrez-Barragan et al., 2022)	7.0T Scanner, RARE image: 0.23×0.23×0.6mm EPI image: 0.23×0.23×0.6mm or 0.2×0.2×0.5mm	Male, C57BL/6J mice. awake group:10 halothane group:14; medetomidine-isoflurane:19	No anesthesia in awake group	26days. 3sessions of mock scanning(5days/sessions). 10min in the first day and up to 32min	Headpost, back and tail were gently taped. Cotton rolls were used to reduce jaw and forepaw	no	Corticosterone, body-weight tracking, open field behavioral test.	Frame-wise displacement for motion evaluation	Resting-state
(Zeng et al., 2022)	14.1T Scanner RARE image: 0.125×0.125×0.5 mm EPI image: 0.3×0.3×0.5 mm	C57BL/6 mice 9 male	no	5-8 weeks. 10–15 min/day to 60 min periodically, 1–2 days of rest after each training session	Headpost	no	Pupil dynamics, behavior monitor	Chest movement, frame-wise displacements (FD) for motion evaluation	Visual stim
(Fadel et al., 2022)	9.4T Scanner T2W image: 0.156×0.156×1.0 mm EPI image: 0.25×0.25×0.6 mm	C57BL/6, 11 mice (5male 5 female)	0.5-1.0% isoflurane	5days, 10mins up to 50mins	tooth bar, nose cone, pieces of gauze were placed to secure the head and body. Tail and feet were tapped	Tooth bar, gauze was placed to fix the head.	corticosterone	Temperature probe was inserted and Respiration	Resting-stae
(Cover et al., 2021)	9.4T Scanner T2W image: 0.117×0.117×0.6 mm EPI image: 0.26×0.26×0.6 mm	C57BL/6, 15 mice (5 failed)		26days, viral injection and water restriction(1week)	fiber ferrule, headpost, acrylic body tube, treadmill	no	no	frame-wise displacements (FD) for motion evaluation	intracranial self-stimulation (ICSS) with optogenetics
(Boch et al., 2021)	3.0T Scanner T2W image: 0.7 mm isotropic EPI image: 1.5×1.5×2.0 mm	31 dogs	unknown	~25 weeks	earplugs, head bandage	ear padding	Pupil dynamics	Frame-wise displacement for motion evaluation	Flickering checkerboard and Face processing experiment
(Dinh et al., 2021)	9.4T Scanner, FLASH Image: 0.059×0.059×0.5mm EPI image: 0.156×0.1456×0.5mm	C57BL/6 mice, 13 male	1% isoflurane before training and imaging	10days, 30min up to 120min, 15min/day increment, for remaining 3days, four mice trained in mock scanner, 3 mice trained in real scanner	Headpost, Body/neck restrain, nose cone	Unknown	Unknown	Respiration Temperature Chest movements were monitored frame-wise displacements (FD) for motion evaluation	Visual stim
(Tsurugizawa et al., 2020)	4.7T Scanner, Anat. Image: 0.125×0.125×1.0mm EPI Image: 0.2×0.2×1.0mm	15q dup mice, 25 mice were used for fMRI (including 10 wide type for control)	2% isoflurane before training and imaging	4days, 2 days outside scanner, 2 days inside scanner. 30min at 1st and 60min at 2nd.	Headpost nose mask ear bar	Ear bar	corticosterone	Heart rate respiration rate Six motion parameters (three translation and three rotation)	olfaction stim
(Chen et al., 2020)	9.4T Scanner, RARE Image:	C57BL/6 mice 40 male	Unknown	7days, day1-day4 head fixed with noise,	Head holder Kwil-cast	Ear is fill with the silicone	Unknown	respiratory ate	Whisker auditory olfactory

	0.0625×0.0625×0.4mm EPI Image: 0.15×0.15×0.4mm 0.1×0.1×0.3mm 0.2×0.2×0.3/0.4mm			Day5-day7 with sensory stimulus	Earphone tube				
(Behroozi et al., 2020)	7.0T Scanner, RARE Image: 0.23×0.23×0.25mm	Pigeons Twenty adult Columba livia	Unknown	3weeks, 10min up to 100 min. Water deprivation for the whole night before the imaging	plastic pedestal, head screws, piezo-electric pressure sensors measuring the dynamic pressure of jaw movements	Unknown	Corticosterone (ACTH stimulation test)	Respiration rate heart rate	color discrimination for Go/no Go task
(Prichard et al., 2020)		dog							
(Karl et al., 2020)		dog							
(Desjardins et al., 2019)	7.0T Scanner, RARE Image: 0.078×0.039×1.0mm EPI Image: 0.2×0.2×1.0mm	C57BL/6J, JAX014548, JAX 005628, JAX 024109, 16 mice	Anesthetize(<60s) for head fixation	2 hours/day	Headpost	Ear plugs	Unknown	Camera surveillance	Whisker optogenetic
(Han et al., 2019)	9.4T Scanner, RARE Image: 0.0625×0.0625×0.4mm EPI Image: 0.15×0.15×0.4mm	C57BL/6J mice 8 male	Unknown	water restriction habituation, automatic lick teaching, automatic shaping, GNG task training	Head holder Kwil-cast	The drum membrane of the middle ear was punctured quickly, and the Kwik-cast was then injected	Unknown	Unknown	olfaction stim for Go/noGO licking
(Matsubayashi et al., 2018)	7.0T Scanner; RARE Image: 0.075×0.075×0.3mm, EPI Image: 0.2×0.2×0.5mm	C57BL/6J mice 9 female	Unknown	5 weeks,2 hours/day, mice underwent laminectomy at the level of the Th9/10 vertebra	Head bar Body restrain	Unknown	Unknown	respiration rate	Unknown
(Takata et al., 2018)	7.0 T Scanner, RARE Image: 0.075×0.075×0.3mm, EPI Image: 0.2×0.2×0.5mm.	Double transgenic mice 22 male 29 female	Unknown	7 days, 2 hours/day	optical fiber head-holder	Unknown	Unknown	Unknown	Optogenetics in the left visual cortex
(Stenroos et al., 2018)	7.0 T Scanner, Anat. Image: 0.097×0.097×0.75mm, EPI Image: 0.39×0.39×1.5mm.	rat 8 male	1.5-2% isoflurane before training and imaging	10 days, 15min up to 45min, forepaws were attached with masking tape, hind paws were tied together with the tail with tape	Body restrain with cloth	bite bar shoulder support pad cheek support nose cone	corticosterone	heart rate respiration	None
(Paasonen et al., 2018)	7.0 T Scanner, Anat. Image: 0.097×0.097×0.75mm, EPI Image: 0.39×0.39×1.5mm.	rat 8 male	1.5-2% isoflurane before imaging	10 days, 15min up to 45min, forepaws were secured and hindpaw with tail were secured using masking tape. The body was wrapped with plastic foam sheet	Body restrain with cloth	bite bar shoulder support pad cheek support nose cone Silicone plugs were inserted into the ear	corticosterone	Unknown	None
(Matsubayashi et al., 2018)	7.0T Scanner, RARE Image: 0.075×0.075×0.3mm, EPI Image:	C57BL/6J mice spinal cord injury 9 female	Unknown	1 week, 2hurs/day	head-bar	Unknown	Unknown	respiration	None

	0.2×0.2×0.5mm.								
(Ma et al., 2018)	7.0T Scanner, Anat. Image: 0.125×0.125×1.0mm, EPI Image: 0.5×0.5×1.0mm.	rat 59 male	3% isoflurane before imaging	7 days	bite bar, ears secured by two adjustable ear pads, and nose secured by a nose bar, head restrainer	Bite bar Ear bar Nose bar	Unknown	translational movement	None
(Smith et al., 2017)	4.7 T Scanner, RARE Image: 0.125×0.125×1.0mm, EPI Image: 0.5×0.5×1.0mm.	Long Evan rats 42 male	2% isoflurane before training and imaging	7days	Headpost, Body restrain	Unknown	Unknown	Unknown	Nome
(Madularu et al., 2017)	7.0T Scanner, RARE Image: 0.3×0.3×1.2mm, Func. Image: 0.3×0.3×1.2mm.	C57BL/6 mice 33 male	2% isoflurane before training and imaging	5 days	No headpost, 3D printed restrain system.	Unknown	Respiration rate, Fecal boli	Volume displacement	olfactory stimulus
(Chang et al., 2017)	7.0 Scanner, Anat. Image: 0.38×0.38×0.5mm, EPI Image: 0.38×0.38×0.5mm.	rats 22 male	Unknown	2 weeks, 30mins/day	Head-Post	Unknown	no	respiratory rates	air-puff stimuli to the side surface of their hind paw
(Poirier et al., 2017)	4.7 scanner, RARE image: 0.125×0.125×1.0mm, EPI image: 0.5×0.5×1.0mm.	adolescent spontaneously hypertensive rat(n=26), Wistar Kyoto(n=20) and Sprague–Dawley(n=12)	1% isoflurane before training and imaging	8 days, 15mins up to 90min, 15 min/day increment	No headpost head restrainer body tube	Ear bar nose clamp	Unknown	Unknown	None
(Van Ruijssevelt et al., 2017)	7.0T Scanner, EPI Image: 0.25×0.25×0.75mm, RARE Image: 0.07×0.07×0.07mm.	zebra finches 10 male	Unknown	25days, 10min up to120min	Head fixed, Body jacket, beak mask and fixation tape.	Unknown	Unknown	Respiration rate	Auditory Stimulus
(Berns et al., 2017)	3.0T Scanner, Anat. Image: 3.0×3.0×2.5mm, Func. Image: 3.0×3.0×2.5mm.	Dog 43 both male and female	Unknown	2 months, 10-15min/day, three days/week,	Unknown	Unknown	Unknown	Unknown	hand signals indicating
(Behroozi et al., 2017)	7.0T Scanner, EPI Image: 0.15×0.15×0.3mm, RARE Image: 0.47×0.47×1.0mm.	Pigeon 8 Valencian Figurita	Unknown	10days, 15min up to 60min	plastic pedestal	Unknown	Unknown	Respiration rate	no
(Yee et al., 2016)	7.0T Scanner, RARE Image: 0.097×0.097×0.7mm EPI Image: 0.26×0.26×0.7mm	prairie voles 14 male	Unknown	no training procedures, only restrain in the scanner	Body restrain and nose cone, bite bar, helmet	Bite bar	Unknown	Heart rate	CO2 (5%) odor
(Moore et al., 2016)	7.0T Scanner, RARE Image: 0.097×0.097×0.75mm, EPI Image: 0.26×0.26×0.75mm.	Male Oprm1+/+ and Oprm1−/− mice	2-3% isoflurane before training and imaging	4 consecutive days, 30min/day	head in a cushion, ear bars, pressure points used to immobilize the head	Ear bar	Unknown	Unknown	5% carbon dioxide
(Madularu et al., 2016)	7.0T Scanner, RARE Image: 0.11×0.11×0.75mm	OVX Sprague Dawley 36 rats	2-3% Isoflurane before training and imaging	5 consecutive days, 30mins/day	head in a cushion, pressure points used to immobilize the	Ear bar	Unknown	Unknown	None

	EPI Image: 0.3125×0.3125×0.75mm				head, ear bars,				
(Kenkel et al., 2016)	7.0T Scanner, RARE Image: 0.11×0.11×1.0mm, EPI Image: 0.3125×0.3125×1.0mm	Adult WT (12) and Fox (10) male Sprague Dawley rats	2-3% Isoflurane before training and imaging	4-5 consecutive days, 30mins/day	Head holder and body tube, no headpost, ear bars, body, paws were tighten in the scanner.	Ear bar	Unknown	Unknown	odor stimulus
(Chang et al., 2016)	7.0T Scanner, EPI Image: 0.38×0.38×0.5mm	Sprague-Dawley rats, 10 male	Unknown	8-10 days, (30min/day)	Headpost, body restrain	Unknown	corticosterone	Respiration rate	Air-puff to the forepaw
(Yoshida et al., 2016)	7.0T Scanner, EPI Image: 0.2×0.2×0.5mm	C57BL/6 mice, 8 male	Unknown	8 days, 2 hours/day	head bar EMG electrodes	Unknown	ECG EMG	Heart rate	None
(Aksenov et al., 2016)	9.4T Scanner, EPI Image: 0.375×0.375×1.0mm	Dutch-belted rabbit 6 female	Unknown	3-5day, restrained by means of a cloth sleeve	headbolts, electrodes and cannulae were implanted	Unknown	LFP MUA	Unknown	Optogenetic Whisker stimulus
(Madularu et al., 2015)	7.0T Scanner, RARE Image: 0.11×0.11×1.0mm EPI Image: 0.3125×0.3125×1.0mm	OVX Sprague Dawley rats 27 female	2-3% Isoflurane before training and imaging	5 consecutive days, 30mins/day	head in a cushion ear bars, pressure points used to immobilize the head	Ear bar	Unknown	Unknown	drug model
(Liang et al., 2015b)	7 T Scanner, RARE Image: 0.125×0.125×1.0mm EPI Image: 0.5×0.5×1.0mm	11 rats	2% Isoflurane before training and imaging	7 days , 15min up to 90min	four plastic MR compatible screws were fixed into the skull, optic fiber was embedded	Ear bar	Unknown	Unknown	Optogenetics
(Liang et al., 2015a)	4.7 T Scanner, RARE Image: 0.125×0.125×1.0mm EPI Image: 0.5×0.5×1.0mm	Long Evan (LE) rats 42 male	2% Isoflurane before training and imaging	7 days, 15min up to 90min	Plexiglas stereotaxic head holder, plastic ear bars, forepaw and hindpaw were loosely taped	Ear bar	Unknown	Unknown	None
(Harris et al., 2015)	7.0 T Scanner, RARE Image: 0.1×0.1×0.8mm EPI Image: 0.3×0.3×0.8mm	C57bl/6 mice 44 male	1–2% Isoflurane before training and imaging	5 days, 22min/day, 12-day protocol 6 min up to 22 min	No headpost, limbs were tapped, body were restrained in the body restrainer, nose cone, foam headband	Foam headband into the ear	respiration rate, heart rate, body movements e.g. leg kicks, arched back) body weight, Corticosterone	Respiration, Heart rate, Body weight, Body movements, Corticosterone,	cued fear conditioning Foot shock(0.5mA)
(Dilks et al., 2015)	3.0T Scanner, Anat. Image: 1.5×1.5×2.0mm, EPI Image: 3.0×3.0×3.0mm.	8 Dogs	None	2-3 months, presentation of images on a computer screen	Unknown	Unknown	Unknown	Unknown	Face processing
(Liang et al., 2014)	4.7 T Scanner, RARE Image: 0.125×0.125×1.0mm EPI Image: 0.5×0.5×1.0mm	Long-Evans (LE) adult rats 32 male	2% Isoflurane before training and imaging	7 days, 15min up to 90min	Plexiglas stereotaxic head holder plastic ear bars, forepaw and hindpaw were loosely taped	Ear bar Bit bar	anxiety level of rats was assessed by using the EPM test	EPM test	None
(Ferris et al., 2014)	7.0 T Scanner, RARE Image: 0.097×0.097×0.75mm, EPI Image: 0.26×0.26×0.75mm.	Wild-type mice (C57B/L6J) (n =5 male, 6 female) and knock in zQ175 HET (n =4 male, 6 female)	2-3% Isoflurane before training and imaging	4 consecutive days, 30min/day	Body tube, nose cone, hollow tube	Bite bar	Unknown	displacement	Odor stimulus

		and HOM (n =5 male, 5 female) mice							
(Ma et al., 2013)	3.0 T Scanner, RARE Image: 0.5×1.0×0.5mm, EPI Image: 2.0×2.0×2.0mm.	4 cats	Unknown	Unknown	head-post, animal chair,	Unknown	Unknown	displacement	Visual stimulus
(Johnson et al., 2013)	7.0 T Scanner, Anat. Image: 0.11×0.11×1.0mm, Func. Image: 0.46×0.46×1.0mm.	Sprague–Dawley rats 9 male	Unknown	10 days cocaine + odor versus no cocaine + no odor training	Chamber, Electrode, intravenous catheters,	Unknown	Unknown	Unknown	cocaine-associated odor cue
(De Groof et al., 2013)	7.0 T Scanner, Anat. Image: 0.085×0.085×0.17mm, Func. Image: 0.34×0.34×1.0mm.	Pigeons 4 adult	None	three distinct procedures: a)10-30-60min for 3days, b)head fixed 10-20-40min,c) with sounds for 1 week	Cloth jacket, head pedestal; plastic tube;	Unknown	Unknown	displacement	visual stimuli
(Berns et al., 2013)	3.0 T Scanner, Anat. Image: 1.5×1.5×2.0mm, Func. Image: 3.0×3.0×3.0mm.	15 dogs	None	2-3months	chin rest, neck coil	Unknown	Unknown	Unknown	Hand signals
(Tsurugizawa et al., 2012)	4.7 T Scanner, Anat. Image: 0.54×0.54×1.3mm, Func. Image: 0.27×0.27×1.3mm.	Wistar rats 12 male	2% isoflurane	3 days, 30-90min	Body restraint, head positioner elastic bands	earplugs	Heart rate respiration rate	Unknown	light stimulation
(Desai et al., 2011)	9.4 T Scanner, Anat. Image: 0.78×0.78×0.5mm, Func. Image: 0.1×0.1×0.5mm, 0.2×0.2×0.5mm.	11 wild-type, 11 transgenic ChR2 mice	0.7% isoflurane for awake imaging	3 days, 20-40mins	Headpost, body restraint tube	Unknown	respiration rate	respiration displacement	optogenetics
(Liang et al., 2011)	4.7 T Scanner, Anat. Image: 0.125×0.125×1.0mm, Func. Image: 0.5×0.5×1.0mm.	Long–Evans rat 16 adult male	isoflurane	8days, 15-90mins	head holder using plastic ear-bars	Ear bar Bite bar	Unknown	Unknown	None
(Zhang et al., 2010)	4.7T Scanner, RARE Image: 0.125×0.125×1.0mm, EPI Image: 0.5×0.5×1.0mm.	Long-Evans (LE) rat 8 adult male	2% Isoflurane before training and imaging	8day, 15min up to 90min	Plexiglas stereotaxic head holder plastic ear bars, forepaw and hindpaw were loosely taped	Ear bar	Unknown	Unknown	None
(Chen et al., 2009)	4.7T Scanner, RARE Image: 0.117×0.117×1.0mm, EPI Image: 0.468×0.468×1.0mm.	8 female rats	2% Isoflurane	3day	Restrainer, headpiece, ear bar, head holder, bite bar, body tube	Ear bar Bite bar	None	None	water (no odor), lemon scent, and TMT odor
(Febo et al., 2008)	4.7T Scanner, RARE Image: 0.117×0.117×1.2mm, EPI Image: 0.468×0.468×1.2mm.	Virgin Sprague-Dawley rats	2-3% isoflurane	4day, 90min/session	Headpiece, head holder, Bite bar, ear bar,	Ear bar Bite bar	None	None	Pup Suckling
(Ferris et al., 2008)	4.7T Scanner, RARE Image: 0.117×0.117×1.2mm,	Adult male and female Long-Evans rats	2–3% isoflurane	4day, 60min/session	Headpiece, head holder, Bite bar, ear bar,	Ear bar	None	displacement	Drug (SRX251 or fluoxetine)

	EPI Image: 0.468×0.468×1.2mm.								
(Duong, 2007)	4.7T Scanner, RARE Image: 0.156×0.156×1.5mm, EPI Image: 0.3125×0.3125×1.5mm.	7 Sprague–Daley rats	2% isoflurane	Unknown	restrained with ear-, nose-, tooth-, and shoulder-bars, and a body restraining tub	restrainer with ear-, nose-, tooth-, and shoulder-bars, and a body restraining tub	Respiration rate Heart rate blood pressure	Respiration rate Heart rate blood pressure	Hypoxia
(Chin et al., 2006)	4.7T Scanner, Anat. Image: 0.156×0.156×1.25mm, Func. Image: 0.156×0.156×1.25mm.	Adult male Sprague-Dawley rats	~3% isoflurane	4day, 7min up to 60min	Training holder, body tube and headpiece	Unknown	None	None	pharmacological (apomorphine and ABT-594)
(King et al., 2005)	4.7T Scanner, RARE Image: 0.1×0.1×1.5mm, EPI Image: 0.2×0.2×1.5mm.	Sprague–Dawley rats 8 male	ketamine and medetomidine being secured	8 consecutive days, 90min/session	headpiece with blunted ear, bite bar, body tube	headpiece with blunted ear, bite bar, body tube	respiratory rate and heart rate corticosterone	corticosterone	None
(Febo et al., 2004)	4.7T Scanner, Anat. Image: 0.117×0.117×1.2mm, EPI Image: 0.468×0.468×1.2mm.	Male Sprague-Dawley rats	2% isoflurane	3-4 days, 90mins/session	cylindrical head holder, body holder,headpiece, bite bar, ear bar	headpiece, bite bar, ear bar	None	None	cocaine
(Sachdev et al., 2003)	4.7T Scanner, Anat. Image: 0.23×0.23×1.2mm, EPI Image: 0.47×0.47×1.2mm.	Long Evans rats 3 male and 2female	Diazepam injection	Body trainer every day for 1 week. after headpost surgery, re-trained for 1 week	felt sleeve, wrapped in a cotton cloth, inserted to the neck into a Plexiglas tube; Velcro straps	three thread-bearing nylon posts; lightweight masking tape; plastic pipe	Unknown	displacement	Whisker stimulus
(Kenneth Sicard, 2003)	4.7T Scanner, Anat. Image: 0.097×0.097×1.5mm, EPI Image: 0.039×0.039×1.5mm.	Sprague Dawley rats 15	2% isoflurane	None	Secured in a rat restrainer with ear-, nose-, tooth-, and shoulder-bars, a body-restraint tube	Ear bar	blood pressure, heart rate, respiration rate		Hypercapnic (CO2) challenges
(Peeters et al., 2001)	7.0T Scanner, Anat. Image: 0.078×0.156×1.0mm, EPI Image: 0.156×0.312×1.0mm.	6 Wistar rats	5% fluothane, Atropine injection, Mivacurium or α-chloralose	None	plexi stereotactic head holder, incisor bar and earplugs	earplugs	None	EEG recording	Electrical forepaw stimulation
(Wyrwicz et al., 2000)	4.7T Scanner, Anat. Image: 0.156×0.156×2.0mm, EPI Image: 0.935×0.935×2.0mm.	rabbits (New Zealand white (NZW) or Dutch Belted (DB)) 5 female	Unknown	30min/sessions 1 or 2 sessions	Tied at the neck and tail in soft cloth bag and fastened to an acrylic cradle with velcro straps with four restraining headbolts.	None	None	None	Visual stimulation

Reference:

Aksenov, D.P., Li, L., Miller, M.J., Wyrwicz, A.M., 2016. Blood oxygenation level dependent signal and neuronal adaptation to optogenetic and sensory stimulation in somatosensory cortex in awake animals. Eur J Neurosci 44, 2722-2729.
Behroozi, M., Helluy, X., Strockens, F., Gao, M., Pusch, R., Tabrik, S., Tegenthoff, M., Otto, T., Axmacher, N., Kumsta, R., Moser, D., Genc, E., Gunturkun, O., 2020. Event-related functional MRI of awake behaving pigeons at 7T. Nat Commun 11, 4715.
Behroozi, M., Strockens, F., Helluy, X., Stacho, M., Gunturkun, O., 2017. Functional Connectivity Pattern of the Internal Hippocampal Network in Awake Pigeons: A Resting-State fMRI Study. Brain Behav Evol 90, 62-72.
Berns, G.S., Brooks, A., Spivak, M., 2013. Replicability and heterogeneity of awake unrestrained canine FMRI responses. PLoS One 8, e81698.
Berns, G.S., Brooks, A.M., Spivak, M., Levy, K., 2017. Functional MRI in Awake Dogs Predicts Suitability for Assistance Work. Sci Rep 7, 43704.
Boch, M., Karl, S., Sladky, R., Huber, L., Lamm, C., Wagner, I.C., 2021. Tailored haemodynamic response function increases detection power of fMRI in awake dogs (Canis familiaris). Neuroimage 224, 117414.
Chang, P.C., Centeno, M.V., Procissi, D., Baria, A., Apkarian, A.V., 2017. Brain activity for tactile allodynia: a longitudinal awake rat functional magnetic resonance imaging study tracking emergence of neuropathic pain. Pain 158, 488-497.
Chang, P.C., Procissi, D., Bao, Q., Centeno, M.V., Baria, A., Apkarian, A.V., 2016. Novel method for functional brain imaging in awake minimally restrained rats. J Neurophysiol 116, 61-80.
Chen, W., Shields, J., Huang, W., King, J.A., 2009. Female fear: influence of estrus cycle on behavioral response and neuronal activation. Behav Brain Res 201, 8-13.
Chen, X., Tong, C., Han, Z., Zhang, K., Bo, B., Feng, Y., Liang, Z., 2020. Sensory evoked fMRI paradigms in awake mice. Neuroimage 204, 116242.
Chin, C.L., Fox, G.B., Hradil, V.P., Osinski, M.A., McGaraughty, S.P., Skoubis, P.D., Cox, B.F., Luo, Y., 2006. Pharmacological MRI in awake rats reveals neural activity in area postrema and nucleus tractus solitarius: relevance as a potential biomarker for detecting drug-induced emesis. Neuroimage 33, 1152-1160.
Cover, C.G., Kesner, A.J., Ukani, S., Stein, E.A., Ikemoto, S., Yang, Y., Lu, H., 2021. Whole brain dynamics during optogenetic self-stimulation of the medial prefrontal cortex in mice. Commun Biol 4, 66.
De Groof, G., Jonckers, E., Gunturkun, O., Denolf, P., Van Auderkerke, J., Van der Linden, A., 2013. Functional MRI and functional connectivity of the visual system of awake pigeons. Behav Brain Res 239, 43-50.
Desai, M., Kahn, I., Knoblich, U., Bernstein, J., Atallah, H., Yang, A., Kopell, N., Buckner, R.L., Graybiel, A.M., Moore, C.I., Boyden, E.S., 2011. Mapping brain networks in awake mice using combined optical neural control and fMRI. J Neurophysiol 105, 1393-1405.
Desjardins, M., Kilic, K., Thunemann, M., Mateo, C., Holland, D., Ferri, C.G.L., Cremonesi, J.A., Li, B., Cheng, Q., Weldy, K.L., Saisan, P.A., Kleinfeld, D., Komiyama, T., Liu, T.T., Bussell, R., Wong, E.C., Scadeng, M., Dunn, A.K., Boas, D.A., Sakadzic, S., Mandeville, J.B., Buxton, R.B., Dale, A.M., Devor, A., 2019. Awake Mouse Imaging: From Two-Photon Microscopy to Blood Oxygen Level-Dependent Functional Magnetic Resonance Imaging. Biol Psychiatry Cogn Neurosci Neuroimaging 4, 533-542.
Dilks, D.D., Cook, P., Weiller, S.K., Berns, H.P., Spivak, M., Berns, G.S., 2015. Awake fMRI reveals a specialized region in dog temporal cortex for face processing. PeerJ 3, e1115.
Dinh, T.N.A., Jung, W.B., Shim, H.J., Kim, S.G., 2021. Characteristics of fMRI responses to visual stimulation in anesthetized vs. awake mice. Neuroimage 226, 117542.

Duong, T.Q., 2007. Cerebral blood flow and BOLD fMRI responses to hypoxia in awake and anesthetized rats. Brain Res 1135, 186-194.
Fadel, L.C., Patel, I.V., Romero, J., Tan, I.C., Kesler, S.R., Rao, V., Subasinghe, S., Ray, R.S., Yustein, J.T., Allen, M.J., Gibson, B.W., Verlinden, J.J., Fayn, S., Ruggiero, N., Ortiz, C., Hipskind, E., Feng, A., Iheanacho, C., Wang, A., Pautler, R.G., 2022. A Mouse Holder for Awake Functional Imaging in Unanesthetized Mice: Applications in (31)P Spectroscopy, Manganese-Enhanced Magnetic Resonance Imaging Studies, and Resting-State Functional Magnetic Resonance Imaging. Biosensors (Basel) 12.
Febo, M., Segarra, A.C., Tenney, J.R., Brevard, M.E., Duong, T.Q., Ferris, C.F., 2004. Imaging cocaine-induced changes in the mesocorticolimbic dopaminergic system of conscious rats. Journal of Neuroscience Methods 139, 167-176.
Febo, M., Stolberg, T.L., Numan, M., Bridges, R.S., Kulkarni, P., Ferris, C.F., 2008. Nursing stimulation is more than tactile sensation: It is a multisensory experience. Horm Behav 54, 330-339.
Ferris, C.F., Kulkarni, P., Toddes, S., Yee, J., Kenkel, W., Nedelman, M., 2014. Studies on the Q175 Knock-in Model of Huntington's Disease Using Functional Imaging in Awake Mice: Evidence of Olfactory Dysfunction. Front Neurol 5, 94.
Ferris, C.F., Stolberg, T., Kulkarni, P., Murugavel, M., Blanchard, R., Blanchard, D.C., Febo, M., Brevard, M., Simon, N.G., 2008. Imaging the neural circuitry and chemical control of aggressive motivation. BMC Neurosci 9, 111.
Gutierrez-Barragan, D., Singh, N.A., Alvino, F.G., Coletta, L., Rocchi, F., De Guzman, E., Galbusera, A., Uboldi, M., Panzeri, S., Gozzi, A., 2022. Unique spatiotemporal fMRI dynamics in the awake mouse brain. Curr Biol 32, 631-644 e636.
Han, Z., Chen, W., Chen, X., Zhang, K., Tong, C., Zhang, X., Li, C.T., Liang, Z., 2019. Awake and behaving mouse fMRI during Go/No-Go task. Neuroimage 188, 733-742.
Harris, A.P., Lennen, R.J., Marshall, I., Jansen, M.A., Pernet, C.R., Brydges, N.M., Duguid, I.C., Holmes, M.C., 2015. Imaging learned fear circuitry in awake mice using fMRI. Eur J Neurosci 42, 2125-2134.
Johnson, T.R., Smerkers, B., Moulder, J.K., Stellar, J.R., Febo, M., 2013. Neural processing of a cocaine-associated odor cue revealed by functional MRI in awake rats. Neurosci Lett 534, 160-165.
Karl, S., Boch, M., Viranyi, Z., Lamm, C., Huber, L., 2020. Training pet dogs for eye-tracking and awake fMRI. Behav Res Methods 52, 838-856.
Kenkel, W.M., Yee, J.R., Moore, K., Madularu, D., Kulkarni, P., Gamber, K., Nedelman, M., Ferris, C.F., 2016. Functional magnetic resonance imaging in awake transgenic fragile X rats: evidence of dysregulation in reward processing in the mesolimbic/habenular neural circuit. Transl Psychiatry 6, e763.
Kenneth Sicard, Q.S., Mathew E. Brevard, Ross Sullivan, Craig F. Ferris, Jean A. King, and Timothy Q. Duong, 2003. Regional Cerebral Blood Flow and BOLD Responses in Conscious and Anesthetized Rats Under Basal and Hypercapnic Conditions: Implications for Functional MRI Studies.
King, J.A., Garelick, T.S., Brevard, M.E., Chen, W., Messenger, T.L., Duong, T.Q., Ferris, C.F., 2005. Procedure for minimizing stress for fMRI studies in conscious rats. J Neurosci Methods 148, 154-160.
Liang, Z., King, J., Zhang, N., 2011. Uncovering intrinsic connectional architecture of functional networks in awake rat brain. J Neurosci 31, 3776-3783.
Liang, Z., King, J., Zhang, N., 2014. Neuroplasticity to a single-episode traumatic stress revealed by resting-state fMRI in awake rats. Neuroimage 103, 485-491.
Liang, Z., Liu, X., Zhang, N., 2015a. Dynamic resting state functional connectivity in awake and anesthetized rodents. Neuroimage 104, 89-99.

Liang, Z., Watson, G.D., Alloway, K.D., Lee, G., Neuberger, T., Zhang, N., 2015b. Mapping the functional network of medial prefrontal cortex by combining optogenetics and fMRI in awake rats. Neuroimage 117, 114-123.
Ma, M., Qian, C., Li, Y., Zuo, Z., Liu, Z., 2013. Setup and data analysis for functional magnetic resonance imaging of awake cat visual cortex. Neurosci Bull 29, 588-602.
Ma, Z., Ma, Y., Zhang, N., 2018. Development of brain-wide connectivity architecture in awake rats. Neuroimage 176, 380-389.
Madularu, D., Kulkarni, P., Yee, J.R., Kenkel, W.M., Shams, W.M., Ferris, C.F., Brake, W.G., 2016. High estrogen and chronic haloperidol lead to greater amphetamine-induced BOLD activation in awake, amphetamine-sensitized female rats. Horm Behav 82, 56-63.
Madularu, D., Mathieu, A.P., Kumaragamage, C., Reynolds, L.M., Near, J., Flores, C., Rajah, M.N., 2017. A non-invasive restraining system for awake mouse imaging. J Neurosci Methods 287, 53-57.
Madularu, D., Yee, J.R., Kenkel, W.M., Moore, K.A., Kulkarni, P., Shams, W.M., Ferris, C.F., Brake, W.G., 2015. Integration of neural networks activated by amphetamine in females with different estrogen levels: a functional imaging study in awake rats. Psychoneuroendocrinology 56, 200-212.
Matsubayashi, K., Nagoshi, N., Komaki, Y., Kojima, K., Shinozaki, M., Tsuji, O., Iwanami, A., Ishihara, R., Takata, N., Matsumoto, M., Mimura, M., Okano, H., Nakamura, M., 2018. Assessing cortical plasticity after spinal cord injury by using resting-state functional magnetic resonance imaging in awake adult mice. Sci Rep 8, 14406.
Moore, K., Madularu, D., Iriah, S., Yee, J.R., Kulkarni, P., Darcq, E., Kieffer, B.L., Ferris, C.F., 2016. BOLD Imaging in Awake Wild-Type and Mu-Opioid Receptor Knock-Out Mice Reveals On-Target Activation Maps in Response to Oxycodone. Front Neurosci 10, 471.
Paasonen, J., Stenroos, P., Salo, R.A., Kiviniemi, V., Grohn, O., 2018. Functional connectivity under six anesthesia protocols and the awake condition in rat brain. Neuroimage 172, 9-20.
Peeters, R.R., Tindemans, I., De Schutter, E., Van der Linden, A., 2001. Comparing BOLD fMRI signal changes in the awake and anesthetized rat during electrical forepaw stimulation. Magn Reson Imaging 19, 821-826.
Poirier, G.L., Huang, W., Tam, K., DiFranza, J.R., King, J.A., 2017. Awake whole-brain functional connectivity alterations in the adolescent spontaneously hypertensive rat feature visual streams and striatal networks. Brain Struct Funct 222, 1673-1683.
Prichard, A., Chhibber, R., King, J., Athanassiades, K., Spivak, M., Berns, G.S., 2020. Decoding Odor Mixtures in the Dog Brain: An Awake fMRI Study. Chemical Senses 45, 833-844.
Sachdev, R.N., Champney, G.C., Lee, H., Price, R.R., Pickens, D.R., 3rd, Morgan, V.L., Stefansic, J.D., Melzer, P., Ebner, F.F., 2003. Experimental model for functional magnetic resonance imaging of somatic sensory cortex in the unanesthetized rat. Neuroimage 19, 742-750.
Smith, J.B., Liang, Z., Watson, G.D.R., Alloway, K.D., Zhang, N., 2017. Interhemispheric resting-state functional connectivity of the claustrum in the awake and anesthetized states. Brain Struct Funct 222, 2041-2058.
Stenroos, P., Paasonen, J., Salo, R.A., Jokivarsi, K., Shatillo, A., Tanila, H., Grohn, O., 2018. Awake Rat Brain Functional Magnetic Resonance Imaging Using Standard Radio Frequency Coils and a 3D Printed Restraint Kit. Front Neurosci 12, 548.
Takata, N., Sugiura, Y., Yoshida, K., Koizumi, M., Hiroshi, N., Honda, K., Yano, R., Komaki, Y., Matsui, K., Suematsu, M., Mimura, M., Okano, H., Tanaka, K.F., 2018. Optogenetic astrocyte activation evokes BOLD fMRI response with oxygen consumption without neuronal activity modulation. Glia 66, 2013-2023.

Tsurugizawa, T., Tamada, K., Ono, N., Karakawa, S., Kodama, Y., Debacker, C., Hata, J., Okano, H., Kitamura, A., Zalesky, A., Takumi, T., 2020. Awake functional MRI detects neural circuit dysfunction in a mouse model of autism. Sci Adv 6, eaav4520.
Tsurugizawa, T., Uematsu, A., Uneyama, H., Torii, K., 2012. Functional brain mapping of conscious rats during reward anticipation. J Neurosci Methods 206, 132-137.
Van Ruijssevelt, L., Hamaide, J., Van Gurp, M.T., Verhoye, M., Van der Linden, A., 2017. Auditory evoked BOLD responses in awake compared to lightly anaesthetized zebra finches. Sci Rep 7, 13563.
Wyrwicz, A.M., Chen, N., Li, L., Weiss, C., Disterhoft, J.F., 2000. fMRI of visual system activation in the conscious rabbit. Magn Reson Med 44, 474-478.
Yee, J.R., Kenkel, W.M., Kulkarni, P., Moore, K., Perkeybile, A.M., Toddes, S., Amacker, J.A., Carter, C.S., Ferris, C.F., 2016. BOLD fMRI in awake prairie voles: A platform for translational social and affective neuroscience. Neuroimage 138, 221-232.
Yoshida, K., Mimura, Y., Ishihara, R., Nishida, H., Komaki, Y., Minakuchi, T., Tsurugizawa, T., Mimura, M., Okano, H., Tanaka, K.F., Takata, N., 2016. Physiological effects of a habituation procedure for functional MRI in awake mice using a cryogenic radiofrequency probe. J Neurosci Methods 274, 38-48.
Zeng, H., Jiang, Y., Beer-Hammer, S., Yu, X., 2022. Awake Mouse fMRI and Pupillary Recordings in the Ultra-High Magnetic Field. Front Neurosci 16, 886709.
Zhang, N., Rane, P., Huang, W., Liang, Z., Kennedy, D., Frazier, J.A., King, J., 2010. Mapping resting-state brain networks in conscious animals. J Neurosci Methods 189, 186-196.